# A HIGH PEAK POWER, X-BAND GYROKLYSTRON FOR LINEAR ACCELERATORS*

W. Lawson, J. Calame, V. L. Granatstein, P. E. Latham, G. S. Park, M. Reiser, C. D. Striffler, and F. J. Williams
Electrical Engineering Department, University of Maryland, College Park, MD 20742

J. Neilson
Varian Associates, Inc., 611 Hansen Way, Palo Alto, CA 94303

## Abstract

The gyrotron mechanism, which generates coherent radiation at the electron cyclotron frequency, facilitates the use of overmoded cavities and is believed to have excellent potential for development into the high peak power, high gain, efficient amplifier required for a high energy linear accelerator. In this paper, we discuss a 30 MW, 1-2 μs, 10 GHz gyroklystron that is currently under development at the University of Maryland.[1] The 30 MW power level represents an enhancement of almost three orders of magnitude over the current state-of-the-art in gyroklystrons.[2] This enhancement will be achieved by utilizing large beam energies and moderately overmoded cavities ($TE_{01}^{o}$). We present recent progress on the design and construction of all the major subsystems, including the modulator, the Magnetron Injection Gun used to generate a 500 keV, 160 A annular beam, the magnet system, and the gyrotron circuit predicted to achieve conversion efficiencies in the 30%-42% range.

## The Modulator

The electron gun is powered by a line-type modulator similar in design to those used by the SLAC klystrons.[3] Four pulse-forming networks (PFN's) in parallel, each with 9-13 stages (nominally with $L_i$ = 1.4 μH and $C_i$ = 0.014 μF), will be resonantly charged to 46 kV by a dc supply. The PFN's will be switched through two thyratrons to a 22:1 pulse transformer, which will provide the required potential of 500 kV and current of 400 A. Approximately half the available current will be shunted through a compensated resistive divider to provide an intermediate voltage for a modulation anode (mod anode). Adjustment of the number of PFN stages will produce pulse flat tops between 1 and 2 μs. A flat top ripple of less than 1% peak-to-peak will be achieved by PFN inductance tuning. The design repetition rate is 4 pps, appropriate to a proof of principle experiment.

## The Magnetron Injection Gun

The rotating annular electron beam is generated by a double anode Magnetron Injection Gun (MIG).[4] The electrode configuration and axial magnetic field profile are shown in Fig. 1. The zeroth order gun design is provided by a set of adiabatic trade-off equations.[5] Particle simulations with a square mesh, finite difference electron trajectory code[6] are used to minimize the non-ideal gun properties by adjustment of the shapes and locations of the three electrodes. A variable mesh code[7] is used to check the design.

The required beam parameters are shown in Table I. A velocity ratio of $v_\perp/v_z$ = 1.5 is selected as a compromise between the desire for high perpendicular velocity and the need to produce a relatively small axial velocity spread ($\Delta v_z$). The design current for minimum velocity spread is 160 A; the operating current range (current values having $\Delta v_z \leq 10\%$) is 120-240 A. The electrode specifications are given in Table II. The selected cathode radius represents a trade-off between requirements on the peak electric field and on temperature-limited operation. For this design, the peak electric fields are below 100 kV/cm on all surfaces. The cathode loading at 160 A is 40% of the space-charge limited current predicted by simulations.

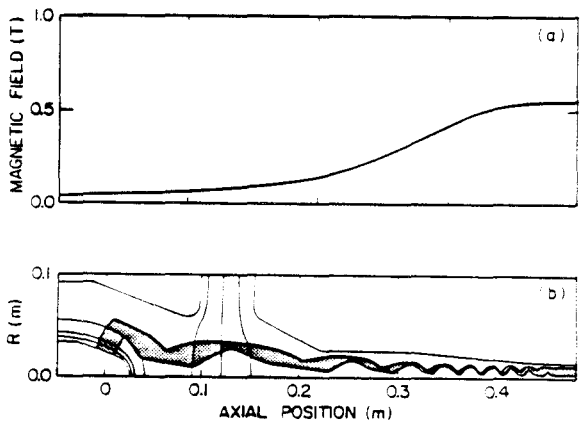


FIG. 1. The magnetron injection gun: (a) the axial magnetic field profile, and (b) the electrode configuration.

Table I. The beam parameters.

| | |
|---|---|
| Beam Power | 80 MW |
| Beam Voltage | 500 kV |
| Magnetic Field $B_o$ | 0.565 T |
| Velocity Ratio $v_\perp/v_z$ | 1.5 |
| Average Guiding Center Radius $r_g$ | 7.85 mm |
| Larmor Radius $r_L$ | 4.29 mm |

The dependence of axial velocity spread on current is shown in Fig. 2. This dependence results from the nonlaminar beam flow (see Fig. 1). The space-charge field generated by the beam increases the perpendicular velocities of electrons emitted from the upper part of the cathode and decreases the perpendicular velocities of the electrons emitted from the lower part of the cathode.[7] This effect counters the initial distribution of perpendicular velocities at the cathode, since the electric field is largest at the minimum radius and the corresponding electrons have the

*This work was supported by the U.S. Department of Energy.

highest velocity ratios. As the current is increased, a minima in velocity spread will occur when the effect of space charge on perpendicular velocity spread best offsets the initial velocity spread at the cathode.

Table II. The electrode specifications.

| | |
|---|---|
| Average Cathode Radius | 22.8 mm |
| Cathode - Mod Anode Gap | 61.3 mm |
| Mod Anode - Main Anode Gap | 55.0 mm |
| Cathode Half-Angle | $20^0$ |
| $B_o/B_{gun}$ | 12 |
| Mod Anode Voltage (Cathode Grounded) | 143 kV |
| Cathode Loading (160 A) | 5.6 A/cm$^2$ |

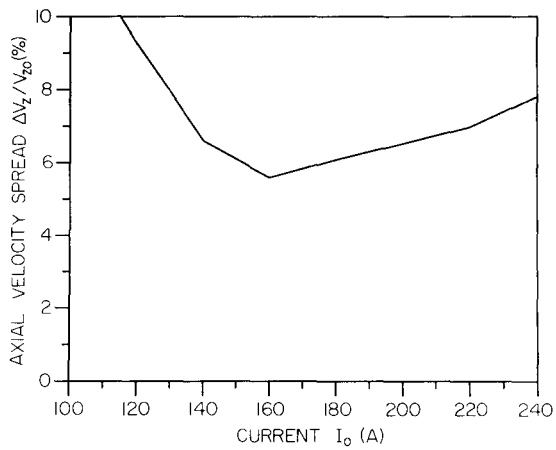


FIG. 2. The range of operating currents.

## The Magnet System

The nominal magnetic field in the microwave circuit region is 0.565 T. This flat field region (< 0.1% variation) is maintained over a 25 cm interval. The magnetic field profile is generated by a set of seven water-cooled pancake coils in the microwave circuit region and supplemented by a large gun coil placed over the cathode and an additional pancake coil placed near the center of the compression region. The length of the compression region, defined as the distance between the emitter strip center and the entrance to the microwave circuit, is 48.25 cm. This is a reasonable compromise between the conflicting requirements of a physically short system and an approximately adiabatic compression. The magnetic field profile is nearly exponential during the first 35 cm of the compression length, which helps reduce the spread in axial velocity. Magnetic field tapering in the circuit region, which is required to optimize efficiency, will be achieved with the use of small trim coils placed near the microwave cavities.

## The Gyroklystron Circuit

A typical gyroklystron circuit is shown in Fig. 3. The primary tool used in the design of the microwave circuit is a partially self-consistent code developed by K. R. Chu.[1] This code finds a steady state solution in each cavity through an iterative algorithm: Maxwell's equations are used to compute the electromagnetic fields from the current while the particle equations of motion are integrated in the fields to compute the current. This loop is iterated until the electromagnetic fields and current are consistent. The cavities are connected by the ballistic beam bunching that occurs in the drift tubes. To achieve a tractable set of equations, a number of simplifying assumptions are made. In particular, we ignore the effects of the beam self fields, and assume a pure mode in the cavities and no fields in the drift tube. With these assumptions, the fields and current are simply related (see, e.g., Eqs. 15 and 17 of Ref. 1), and the simulation of a multivcavity gyroklystron operating in the nonlinear regime may be carried out with reasonable computer resources.

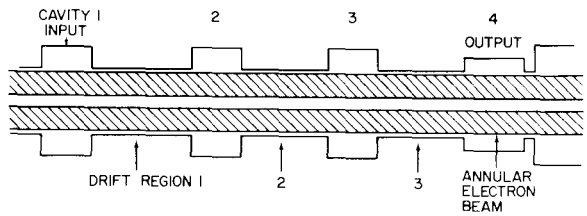


FIG. 3. The four cavity gyroklystron circuit.

Unlike a conventional klystron, the particle bunching is in phase rather than configuration space. For high efficiency operation, the particles must be tightly bunched when entering the last cavity (where energy extraction occurs). There are two factors that determine the final 'size' of a bunch: its spread in energy and spread in phase. To minimize the spread in energy, small fields and long drift tubes may be used. In the absence of a spread in velocity ($\Delta v_z$), such an approach yields a compact bunch. However, even small $\Delta v_z$ causes a spread in phase during ballistic bunching, and can have a large deleterious effect on the final bunch 'size.' In our work, we find the spread in phase due to the finite $\Delta v_z$ to be far more important than the spread in energy. For that reason, we operate with large fields and short drift tubes. The large fields are achieved by operating near start oscillation current, either by raising the cavity Q's or increasing the cavity length. In this way, a reasonably small bunch may be achieved at the entrance to the output cavity. Final optimization of efficiency is done while keeping the average wall loss and the space charge depression within acceptable limits, making sure that no unwanted modes are excited, and operating below the start oscillation current in all cavities.

The optimized circuit values based on the nominal beam parameters (Table I) and the gun simulations are shown in Table III. The required cavity Q's are two orders of magnitude below the wall loss Q's for good conductors. This is convenient for the output cavity where diffractive losses dominate. The microwave power is extracted from an end wall through a coupling aperture. The cold cavity fields are found numerically via truncated sets of the eigenfunctions of a right circular waveguide. Cold tests have verified the theoretical Q's to ± 3% and the theoretical resonant frequencies to ± 0.4%. Frequency tuning can be

achieved by slight adjustments of the axial location of the coupling aperture. The low Q's of the buncher cavities present more of a problem, but several techiques are currently being cold tested. Resonant input coupling techniques are useful because of the narrow band application and are also being cold tested. The drift tubes are not cutoff to the $TE_{11}$ and $TE_{21}$ modes, and provisions must be made to insure stability in those regions. Cold testing has demonstrated that drift tubes comprised of alternative rings of conductor and absorber sufficiently attenuate the $TE_{11}$ mode. The effect of the composite drift tubes on the $TE_{21}$ and $TE_{01}$ modes is currently being studied.

Table III. The optimized circuit values based on the gun simulations.

| Cavity | Length (cm) | Radius (cm) | Q |
|---|---|---|---|
| 1 | 2.22 | 2.48 | 375 |
| 2 | 2.25 | 2.48 | 375 |
| 3 | 2.25 | 2.45 | 375 |
| 4 | 3.00 | 2.11 | 220 |

| Drift Tube | Length (cm) | Radius (cm) |
|---|---|---|
| 1 | 4.50 | 1.50 |
| 2 | 3.90 | 1.50 |
| 3 | 3.90 | 1.50 |

The gain curve at the design current is shown in Fig. 4. The peak power of 33 MW occurs at a gain of 64.1 dB. In Fig. 5, the effect of axial velocity spread on efficiency is demonstrated. At each value of $\Delta v_z$, the magnetic field is adjusted to maximize efficiency. The large signal AM and PM sensitivities to various parameters are listed in Table IV. If the phase shift is to be less than a few degrees, as required for accelerator applications, then the applied magnetic field strength and the beam voltage must be regulated to within a small fraction of a percent, and/or feedback stabilization circuitry must be used.

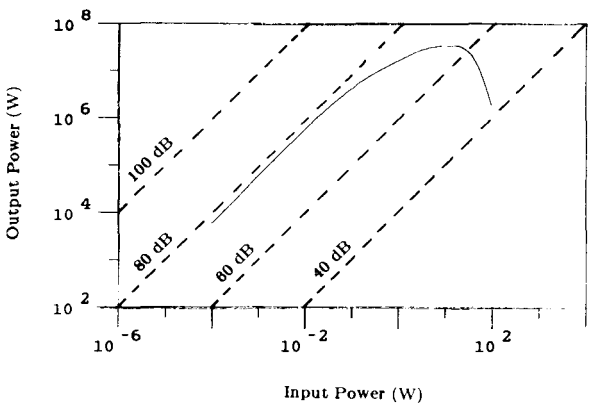


FIG. 4. Output power versus driver power for the optimized operating conditions.

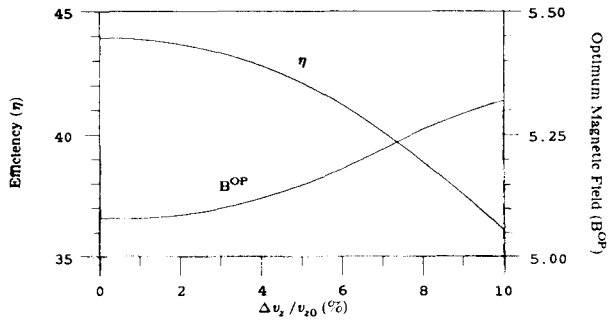


FIG. 5. Large signal efficiency versus axial velocity spread.

Table IV. The large signal AM and PM sensitivities to various parameters.

| Parameter | AM | PM |
|---|---|---|
| Beam Voltage | 0.090 dB/% | $19.0^0$/% |
| Beam Current | 0.075 dB/% | $1.8^0$/% |
| Magnetic Field | 0.037 dB/% | $41.0^0$/% |

## Summary

Current theoretical models indicate that all the design goals can be achieved. The modulator, electron gun, and magnet system have been designed and are currently being constructed. Cold testing of the output cavity has been completed; cold testing of other components is in progress. The circuit simulation is currently being upgraded to include tapered magnetic fields, realistic cold cavity field profiles, and dc space charge effects.

## References

1. K. R. Chu, V. L. Granatstein, P. E. Latham, W. Lawson, and C. D. Striffler, IEEE Trans. Plasma Sci. PS-13, 424-434, (1985).

2. W. M. Bollen, A. H. McCurdy, B. Arfin, R. K. Parker, and A. K. Ganguly, IEEE Trans. Plasma Sci. PS-13, 417 (1985).

3. The Stanford Two Mile Accelerator, edited by R. B. Neal (W. A. Benjamin, Inc., New York, 1968), p. 411.

4. W. Lawson, J. Calame, V. L. Granatstein, G. S. Park, and C. D. Striffler, Int. J. Electron., 4th Special Issue on Gyrotrons, to be published.

5. J. M. Baird and W. Lawson, ibid.

6. W. B. Herrmannsfeldt, "Electron Trajectory Program," SLAC Report-226, November 1979.

7. J. Neilson, M. Caplan, N. Lopez, and K. Felch, 1985 IEDM Tech. Digest, pp. 184-187 (1985).